

STEADY STATE CORE PHYSICS METHODS  
FOR BWR DESIGN AND ANALYSIS

(Appendix F)

January 1992

Principal Engineer

Craig H. Greene

Contributors

Brian J. Boyle  
Jon Juneau  
Lynn A. Leatherwood  
Gary W. Scronce  
Phu Van Vo  
Marcia L. Wittenburg

Review: Lynn A. Leatherwood 1/8/92  
L.A. Leatherwood Date  
Supervisor - Core Analysis

Approve: J.S. Miller 1/8/92  
J.S. Miller Date  
Director - Engineering Analysis

Gulf States Utilities Company  
River Bend Station  
P.O. Box 220  
St. Francisville, Louisiana 70775

IMPORTANT NOTICE REGARDING CONTENTS OF THIS DOCUMENT  
PLEASE READ CAREFULLY

This document was prepared by Gulf States Utilities Company for the use of the U.S. Nuclear Regulatory Commission in matters regarding the operating license for the River Bend Station. To the best of the issuer's knowledge, this document contains work performed in accordance with sound engineering practice and is a true and accurate representation of the facts.

The work reported herein is the property of Gulf States Utilities Company, and any usage other than as described above is prohibited. Other than for the intended usage, neither Gulf States Utilities Company, nor any of its employees or officers, nor any other person acting on its behalf:

- \* Makes any warranty or representation, express or implied, with respect to the accuracy, completeness, or usefulness of the information contained in this report, or that the use of any information, apparatus, method, or process disclosed herein would not infringe privately owned rights; or
- \* Assumes any liabilities with respect to the use of, or for damages resulting from the use of, any information, apparatus, method, or process disclosed in this report.

EA-CA-91-0001-S1  
Revision 0

APPENDIX F  
ADDITIONAL INFORMATION

LIST OF TABLES

<u>Table</u>	<u>Subject</u>	<u>Page</u>
F-4.1	RBS Cold Critical Statepoints . . . . .	13
F-6.1	RBS SLCS Cold Shutdown Margins . . . . .	18
F-6.2	RBS CRWE Analysis . . . . .	19
F-6.3	RBS Cycle 2 LFWH Analysis . . . . .	20
F-15.1	Summary of Quad Cities Critical Predictions . . . . .	38

LIST OF FIGURES

<u>Fig.</u>	<u>Subject</u>	<u>Page</u>
F-14.1	Gadolinia Worth vs Cycle Exposure, RBS Cycles 1-3 . . . . .	34
F-14.2	Critical Eigenvalue vs Gadolinia Inventory, RBS Cycles 1-3 . . . . .	35

APPENDIX F  
ADDITIONAL INFORMATION

Information contained in this Appendix was compiled in response to technical questions arising during the review of the original issue of the base report. The questions contained in this Appendix were transmitted by the technical reviewer<sup>1</sup>.

---

<sup>1</sup>Letter, Douglas V. Pickett (NRC) to James C. Deddens (GSU), "River Bend Station, Unit 1 - Request for Additional Information Concerning Topical Report EA-CA-91-0001-M, Revision-0, 'Steady State Core Physics Methods for BWR Design and Analysis,' (TAC No. M79641)" dated December 9, 1991.

**NRC Question:**

1. Describe the Gulf States Utilities (GSU) modifications to SIMULATE-E (e.g., the TIP model) and the supporting EPRI codes. What modifications were made to the ABLE code?

**GSU Response:**

Printed output for all of the EPRI codes has been modified to include sufficient information to allow full tracing of the software version and specific supporting calculations used for each analysis. Most of this information is passed from one code to another as part of the title string identifying the output. Except as noted in this response, the technical calculation performed by each of the EPRI-provided codes has been retained as originally provided.

SIMULATE-E. GSU technical modifications to SIMULATE-E include modifications to the incore instrument response module, expansion of internal arrays to larger limits, addition of a thermal limits module, and a number of changes implemented for operational support analysis. Some of the changes in the coding were associated with clearer presentation of output data and resolution of computer system specific problems encountered while implementing the code under the IBM MVS/ESA and MVS/XA operating systems.

*Incore Instrument Response Module.* The TIP model was revised to allow assignment of instrument response factors according to lattice type rather than four-assembly configuration type as originally coded. The original TIP model required the generation of polynomial instrument responses for each separate four-bundle configuration surrounding an instrument tube and did not allow axial variation. The revised module calculates the instrument response at each location from the adjacent bundles and combines the contributions to calculate an overall response. The individual bundle response factors are extracted from the CASMO output by AMANDA (see response to Question 3) and converted into general data tables similar to the SIMULATE-E cross section tables.

*Thermal Limits Module.* SIMULATE-E was originally prepared with logical paths to dummy thermal limits routines. GSU added modules to the code which evaluate core performance against operating limits for LHGR, MAPLHGR, and MCPR. Linear heat generation rate (LHGR) is calculated from nodal power and CASMO-derived local peaking factors correlated as functions of exposure, void, and control state. Average planar linear heat generation rate (APLHGR) is calculated at each node from nodal power and assembly geometry. Minimum critical power ratio (MCPR) is calculated using the GEXL-PLUS critical power correlation and algorithm<sup>1</sup>.

*Other Technical Changes.* Existing logic was modified to improve convergence during reactivity search calculations. SIMULATE-E was also modified to implement calculation of rod block limiting percent power at given core conditions, and power weighted k-infinity of each four-assembly rodded and unrodded cell. These calculations were added for operational support and do not contribute to design basis analyses.

NORGE-B. GSU's implementation of NORGE-B has been renamed AMANDA. Modifications to the original coding are described in the response to Question 3.

CASMO. After CASMO was implemented, EPRI provided several technical modifications. GSU implemented these modifications as they were transmitted, resulting in a final software package which included most of the BWR-related additional features of CASMO-2. The EPRI-supplied CASMO improvements included provisions for a depletion calculation of a single pin cell problem, the storing and retrieving of restart files with different passwords, the specification of compositions without having to use the compositions in the material distribution, the addition of editing and punching capabilities, the ability of changing the total number of nuclides used in a dependent case, an increase in array sizes to allow larger problems to be executed, an increase in the number of regions which may be specified for water holes which occupy four pin cell regions, an improvement in boundary condition representation in problems with large flux gradients at the bundle edge, and a correction of a flux normalization error when CASMO is executed without the fundamental mode solution.

---

<sup>1</sup>"GEXL-PLUS Correlation Application to BWR/2-6 Reactors, GE6 Through GE8 Fuel," NEDC-31598P, General Electric Company (1988); proprietary.

To allow evaluation of the relative effects of delayed neutron data from ENDF/B-III and ENDF/B-V separately, provisions were added to allow user input of delayed neutron data. As a part of this modification, the default delayed neutron data were revised to agree with that published in the ENDF/B-V data library. GSU analyses were performed using the revised default delayed neutron data.

MICBURN. No technical changes have been implemented in MICBURN.

ABLE. GSU's modifications to ABLE include thermal-hydraulic modeling of the upper and lower reflector regions, calculation of average neutronic properties of the top and bottom reflectors, and calculation of axially averaged moderator and fuel properties used in the radial reflector calculations. Further discussion of the application of ABLE is contained in the response to Question 2.

**NRC Question:**

2. Describe the ABLE code used for determining the boundary conditions and thermal leakage correction factors. How are the effects of fuel temperature, exposure, voids, rod pattern and core loading accounted for in determining the parameters for a given statepoint? Are these parameters changed during a cycle and/or from cycle to cycle?

**GSU Response:**

ABLE<sup>1</sup> uses one-dimensional, two-group diffusion theory to calculate the two-region reflector boundary conditions for a reactor core. The albedo boundary conditions and the reflector node power correction factor are calculated in ABLE using a method similar to that recommended by Ancona<sup>2</sup>. The ABLE calculation is premised on three major assumptions:

1. The reflector region is an infinite half-plane;
2. The fuel region is an infinite slab with sufficient thickness to make the slab-reflector configuration critical; and
3. Diffusion theory holds in both the fuel and reflector regions.

The ABLE calculation uses two group cross sections in the fuel and reflector regions. The fuel and the radial reflector cross sections are calculated by CASMO, while the top and bottom reflector cross sections are obtained by homogenizing material cross sections in the respective reflectors.

---

<sup>1</sup>B. L. Darnell, B. Morris, M. L. Zerkle, "ABLE: An Albedo Boundary Leakage Evaluation Program for Light Water Reactors; Computer Code User's Manual," Science Applications, Inc. (1984).

<sup>2</sup>A. Ancona, "Reactor Nodal Methods Using Response Matrix Techniques," Ph.D. Thesis, Rensselaer Polytechnic Institute (December 1977), pp. 88-110.

An independent study<sup>1</sup> showed that horizontal albedos are nearly independent of fuel properties. The important parameters in the calculation of albedo boundary conditions are the properties of the moderator. Fuel cross sections used as input to the ABLE code are obtained from CASMO calculations for a representative set of fuel conditions which may be determined from preliminary SIMULATE-E analysis or assumed to be at approximately core average conditions. Since the effects of variations in fuel temperature, exposure, voids, rod pattern and core loading are small, such variations are not considered in the calculation of horizontal or axial albedos.

In the same independent study, thermal leakage correction factors were observed to be dependent on moderator void fraction in the fuel region. This dependence is accounted for by SIMULATE-E through the use of a linear function of the ratio of the group one effective removal cross section to the group two absorption cross section. The linear function is not significantly dependent on fuel type, fuel exposure, fuel temperature or core control rod density.

Originally, the GSU methodology included explicit horizontal albedo factor calculations for each operating cycle. Following detailed calculation of these boundary conditions for the first two RBS core configurations, a sensitivity study indicated that selection of horizontal albedo values had a very small effect on critical eigenvalue and core power distribution beyond the outermost ring of fuel assemblies. Based on the relative insensitivity of the SIMULATE-E results to the albedo values, the choice was made to select a representative set of horizontal albedos and hold them constant for all subsequent operating cycles. Predictions of the first three operating cycles as presented in Appendix C have shown that the eigenvalue and power shape predictions remain consistent despite the use of generalized albedo values.

The Quad Cities and Peach Bottom benchmarks reported in Appendices A and B, respectively, further demonstrate the equivalence of generic and detailed albedos. While both calculations contained explicitly calculated albedos for the first cycle, only the Peach Bottom calculation used explicit albedos for the second cycle. Consistent prediction of

---

<sup>1</sup>A. Ancona, "SIMULATE: BWR Radial Albedo Boundary Condition and Spectrum Correction Factor Verification," *Trans. Am. Nucl. Soc.*, **34** (1980).

individual TIP strings and TIP integrals between the two benchmark calculations further illustrate the lack of sensitivity to detailed albedo calculations.

Upper and lower reflector albedo boundary conditions were initially chosen consistent with recommendations from other SIMULATE-E users. These values were adjusted to provide consistent agreement with Cycle 1 TIP measurements. During the adjustment process, it was observed that the analytical result was relatively insensitive to vertical albedo factors; hence, RBS core follow and design basis analyses use a generalized set of upper and lower albedos which have not been varied from cycle to cycle.

**NRC Question:**

3. Describe the AMANDA computer program used to interface between CASMO and SIMULATE-E.

**GSU Response:**

AMANDA was developed from NORGE-B, which was provided by EPRI to concatenate CASMO output into a format consistent with the SIMULATE-E two-group cross section model. Most of the NORGE-B calculation was retained intact. Modeling differences were implemented in the cold cross section model and the control rod model.

Beyond the capabilities of NORGE-B, AMANDA provides partial cross section tables for samarium, prints k-infinity with and without samarium and xenon, provides data tables for the TIP response constants, provides an accurate representation of the cold rodded absorption cross sections<sup>1</sup>, provides flexibility in the usage of the number of cold void histories and instantaneous temperatures (AMANDA will handle cold cases with 3 void histories and 5 instantaneous moderator densities), and provides the delayed neutron and fission product yields in the SIMULATE-E card image format.

The data tables generated by AMANDA comprise two-dimensional tables and polynomials which provide parametric dependencies on nodal properties tracked by SIMULATE-E. These properties include fuel exposure, moderator void fraction, control rod presence, control history, fuel temperature, and number density of specific fission products. While AMANDA allows specific modeling of samarium, the benchmark analyses in Appendices A-C consider the promethium-samarium chain as part of the lumped fission products which are implicitly included in the base cross section.

---

<sup>1</sup>A. Ancona, "Improved Method for SIMULATE-E Cross-Section Modeling", *Trans. Am. Nucl. Soc.*, 46 (1986).

**NRC Question:**

4. Explain the relatively high cold critical eigenvalues for River Bend Station (RBS) Cycle-2 compared to the cold critical eigenvalues for Cycles 1 and 3.

**GSU Response:**

The average cold critical eigenvalues reported for Cycles 1-3 in Table 6.9 were based on an evaluation of all the statepoints shown in Table 6.10. The average cold critical eigenvalue was to be used as the nominal case for shutdown margin calculations. The database contains a number of statepoints which are inappropriate for use in determination of subsequent cycle cold critical eigenvalues. When the database is reduced to the appropriate points, the three cycles' results are very similar in magnitude.

Critical eigenvalues from specific cold critical statepoints are used to determine an uncertainty factor required for the prediction of subsequent cycle cold critical eigenvalues. Selection criteria for the statepoints include sufficient shutdown time for fission product transients to decay out and moderator pressure and temperature conditions such that localized boiling is not likely. Fission product transients and localized boiling may introduce initial conditions which are outside the modeling assumptions.

The cold critical statepoints from Cycles 1-3 are shown in Table F-4.1. These statepoints were selected from those listed in Table 6.10 by disallowing the statepoints with moderator temperature above 200°F and the statepoints with insufficient shutdown time for xenon decay. The BOC1 analysis which otherwise met the acceptance criteria was also disallowed because sensitivity studies at that point were used to establish the control rod strength adjustment factors used in the analysis.

The eigenvalues from the cold critical statepoints as selected above are characterized by a mean of 1.0106 and a standard deviation of 0.09% $\Delta k$ . The average cold critical eigenvalues for Cycles 1, 2, and 3 are 1.0107, 1.0107, and 1.0102, respectively.

Many of the critical eigenvalues presented in the topical report were for core conditions which do not qualify as cold critical statepoints. Most of these cases were extracted from

operations support calculations used to predict the control rod pattern at cold or warm startup. These other analyses were included in the applications chapter to demonstrate GSU staff's capability to adapt the technology to the operations support mode.

Table F-4.1  
RBS Cold Critical Statepoints

<u>Cycle Exposure (GWd/mt)</u>	<u>Moderator Temperature (°F)</u>	<u>k-effective</u>
<b>Cycle 1 Analysis</b>		
1.384	180	1.01126
3.027	162	1.01017
<b>Cycle 2 Analysis</b>		
0.000	130	1.01171
0.000	195	1.00964
<b>Cycle 3 Analysis</b>		
0.000	152	1.01021

**NRC Question:**

5. How are the calculational uncertainties accounted for in the GSU licensing analyses of the standby liquid control system (SLCS) cold shutdown margin, the control rod withdrawal error (CRWE) analysis and the loss of feedwater heating (LFWH) analysis?

**GSU Response:**

In the application of SIMULATE-E to off-nominal conditions such as SLCS shutdown margin, CRWE analysis, and LFWH analysis, allowance for calculational uncertainties is made in the selection of conservative input conditions for the analysis. Calculational uncertainties are accounted for in these analyses by forcing factors important to the analyses to be in the worst configuration so that any deviations seen in actual plant operation reduce the severity of the event. The use of a bounding analysis assures that the results of the SIMULATE-E calculation are a conservative representation of the anticipated conditions and the appropriate uncertainties.

*SLCS Cold Shutdown Margin.* The analysis for the Standby Liquid Control System is performed at cold (68°F), xenon-free conditions with all rods out at the cycle exposure with the highest cold excess reactivity. Consistent with the plant Technical Specifications, the final boron concentration attained by the system is assumed to be 660 ppm, which is substantially lower than the design specification (and expected system performance) of 825 ppm. The SIMULATE-E model is set up with a conservative value of liquid boron cross section.

*CRWE Analysis.* The core configuration selected for the Control Rod Withdrawal Error analysis represents a major departure from normal operation of the reactor core. The conservative conditions for this analysis include the choice of an unrealistically conservative control rod pattern which places a high worth bundle (*i.e.*, one close to the LHGR, MAPLH and MCPR operating limits) near a high worth control rod. Further conservatism is introduced by ignoring the Rod Pattern Controller, which prevents the implementation of a configuration which includes a high-worth control rod below the Low Power Setpoint, and the Rod Withdrawal Limiter, which stops control rod

movement after two feet of withdrawal. This conservative approach to the CRWE analysis assures that any actual error in control rod operation will cause thermal margin consequences which are bounded by the results of the calculation.

*LFWH Analysis.* The maximum number of feedwater heaters which can be tripped or bypassed by a single event represents the most severe transient for analysis considerations. This event has conservatively estimated to incur a loss of up to 100°F of the feedwater heating capability of the plant and corresponding increase in core inlet subcooling. The pre-transient power level is chosen to be 102% instead of 100% of rated thermal power to bound the initial reactor statepoint. The high simulated thermal power trip scram is assumed to be inoperable. This scram would normally act to prevent reactor power from reaching a post-transient power level consistent with a 100°F reduction in feedwater temperature. The changes in power and MCPR resulting from the transient are larger in the analysis than would otherwise be observed. In addition, the analysis is performed such that fuel exposure related effects such as reactivity coefficients are accounted for.

**NRC Question:**

6. Have GSU calculations been performed for the SLCS cold shutdown margin and the CRWE and LFWH events for RBS Cycles 1 and 2? If so, how do the results compare with the vendor's predictions?

**GSU Response:**

GSU calculations for the SLCS, CRWE and LFWH analysis have also been performed for RBS Cycles 1 and 2. The results of these analyses and corresponding fuel vendor results are contained in this response.

In the fuel vendor calculations, Cycle 2 and 3 analyses were performed in advance on the basis of predicted end of cycle exposure. The GSU calculations were performed on the basis of actual end of cycle exposure. Plant operation for the first two operating cycles was extended slightly beyond the projected nominal end of cycle, resulting in GSU analyses with a slightly less reactive core than the one modeled in the fuel vendor analyses. For applications using SIMULATE-E, this difference translates into slightly less severe transient effects.

*SLCS Cold Shutdown Margin.* GSU and fuel vendor analytical results for the SLCS shutdown margin evaluation for RBS Cycles 1 and 2 are summarized in Table F-6.1. In this table the SLCS shutdown margin calculation results are presented for the minimum shutdown margin verified at actual BOC conditions, and the shutdown margin predicted by the fuel vendor.

The difference between GSU-calculated shutdown margins and those calculated by the fuel vendor are attributed mainly to differences in conservatism included in the modeling assumptions; for example, in Cycle 1 the fuel vendor assumed that the rodged unborated eigenvalue is the eigenvalue to be used in determining a conservative value for the SLCS shutdown margin. The GSU and fuel vendor results would have agreed more closely if both analyses had been best estimate.

*CRWE Analysis.* The results of CRWE analyses for Cycles 1-3 are summarized in Table F-6.2. The Cycle 1 and 2 analyses differ from the Cycle 3 analysis included in the

original submittal in that the limiting control rod pattern was taken from fuel vendor results rather than determined analytically. The Cycle 3 analysis demonstrated the methodology's ability to predict the same limiting control rod pattern as the fuel vendor methodology.

*LFWH Analysis.* Results of GSU's calculation of the LFWH transient for Cycle 2 conditions are summarized in Table F-6.3. As was observed for Cycle 3 conditions, the  $\Delta$ CPR calculated by GSU was slightly lower than the fuel vendor calculation. This difference is due in part to a slightly different final power level calculated by the two different computer codes. When the final power level calculated by the fuel vendor's nodal simulator code is substituted for the power search calculation in SIMULATE-E, the  $\Delta$ CPR values agree closely between GSU and fuel vendor results. The difference is compounded by the initial MCPR values in the analysis; higher initial MCPR values generally result in greater  $\Delta$ CPR values, and the fuel vendor analysis begins with a higher MCPR.

Comparative calculations for Cycle 1 were not performed because the fuel vendor used a point kinetics transient model to analyze the event.

Table F-6.1  
RBS SLCS Cold Shutdown Margins

	<u>GSU Analysis</u>	<u>Fuel Vendor</u>
<b>Cycle 1 Analysis</b>		
Critical Eigenvalue <sup>1</sup>	0.99960	0.99740
Borated Eigenvalue	0.91663	0.93922 <sup>2</sup>
$\Delta K/K$	0.083	----
$\Delta K/K$ exposure corr. <sup>3</sup>	-0.000	----
SLCS Shutdown Margin	0.083	0.058
<b>Cycle 2 Analysis</b>		
Critical Eigenvalue	1.01171	0.99900
Borated Eigenvalue	0.94189	0.95645 <sup>4</sup>
$\Delta K/K$	0.069	----
$\Delta K/K$ exposure corr. <sup>3</sup>	-0.008	----
SLCS Shutdown Margin	0.061	0.043
<b>Cycle 3 Analysis</b>		
Critical Eigenvalue	1.01021	0.99900
Borated Eigenvalue	0.96546	0.96890 <sup>5</sup>
$\Delta K/K$	0.044	----
$\Delta K/K$ exposure corr. <sup>3</sup>	-0.000	----
SLCS Shutdown Margin	0.044 <sup>6</sup>	0.030

<sup>1</sup>The critical eigenvalue is the actual model eigenvalue at the specific BOC condition.

<sup>2</sup>ARI eigenvalue assumed as a conservative substitute for the borated eigenvalue.

<sup>3</sup>This is the exposure correction required to determine the shutdown margin at the cold peak excess reactivity point.

<sup>4</sup>Borated eigenvalue at 660 ppm assumed to be 0.01 lower than calculated borated eigenvalue at 600 ppm, which was 0.96645 for Cycle 2.

<sup>5</sup>Borated eigenvalue at 660 ppm assumed to be 0.01 lower than calculated borated eigenvalue at 600 ppm, which was 0.9789 for Cycle 3.

<sup>6</sup>This implied shutdown margin at BOC3 verifies the original 0.042 shutdown margin which was based on the Cycle 3 cold predicted critical eigenvalue.

Table F-6.2  
RBS CRWE Analysis

	<u>GSU Analysis</u>	<u>Fuel Vendor Analysis</u>
	<b>Cycle 1 Analysis</b>	
Limiting pull OLMCPR	12 to 16 1.12	12 to 16 1.15 <sup>1</sup>
	<u>GSU Analysis</u>	<u>Fuel Vendor Analysis</u>
	<b>Cycle 2 Analysis</b>	
Limiting pull OLMCPR	12 to 16 1.16	12 to 16 1.16 <sup>1</sup>
	<u>GSU Analysis</u>	<u>Fuel Vendor Analysis</u>
	<b>Cycle 3 Analysis</b>	
Limiting pull OLMCPR	08 to 12 1.16	08 to 12 1.18 <sup>2</sup>

---

<sup>1</sup>GE methodology used GEXL. GSU uses GEXL-PLUS, improved methodology.

<sup>2</sup>GEXL-PLUS methodology used by vendor and GSU.

Table F-6.3  
RBS Cycle 2 LFWR Analysis

Parameter	<u>GSU Analysis</u>	<u>Fuel Vendor Analysis</u>
Core Power (% of rated)		
Beginning	102.0	102.0
Ending	114.3	116.3
Eigenvalue		
Beginning	0.99401	0.99782
Ending	0.99411	0.99780
Core Inlet Subcooling (BTU/lbm)		
Beginning	23.3	23.3
Ending	38.8	39.5
Maximum Fraction of Limiting Power Density		
Beginning	0.801	0.772
Ending	0.960	0.948
Minimum Critical Power Ratio		
Beginning	1.220	1.343
Ending	1.157	1.256
$\Delta$ CPR	0.06	0.09

**NRC Question:**

7. How is the feedwater temperature reduction in the LFWH event related to the core inlet subcooling used in the SIMULATE-E LFWH analysis?

**GSU Response:**

Core inlet subcooling is defined as the difference in enthalpy between the fluid entering the active core region and the saturation enthalpy at the core pressure. Factors influencing the core inlet subcooling are the core pressure, the core flow rate, the feedwater flow rate, and the feedwater temperature.

The critical eigenvalue for the LFWH analysis is calculated at 102% power and 100% flow. At these conditions, RBS feedwater heaters are observed to provide feedwater to the plant at a temperature of 422.9°F. Core inlet subcooling is determined by heat balance at the power, flow, and feedwater temperature mentioned above.

To determine the perturbed state, feedwater temperature is reduced by 100°F. A heat balance is used to determine initial values of core pressure and inlet subcooling at a perturbed power level estimated to correspond to the reduction in feedwater temperature. Search logic in SIMULATE-E is used to determine a power level which matches the critical eigenvalue when the newly calculated pressure and subcooling are used. Core pressure and inlet subcooling are recalculated at the new power level, and the perturbed state calculation is iterated until the core inlet subcooling and power converge.

**NRC Question:**

8. How are the system variables (flow, pressure, etc.) determined during the LFWH event? Discuss any approximations made in this determination and how the resulting uncertainties are accounted for.

**GSU Response:**

Feedwater system performance is assumed consistent with plant performance measurements. Feedwater temperature is conservatively assumed to decrease by 100°F from the nominal value from the loss of feedwater heating.

Feedwater flow and steam flow are expected to increase slightly as power increases during the event, so these variables are recalculated in the heat balance for use in the SIMULATE-E perturbed state power calculation. Iodine and xenon concentrations are established at the 102% power, 100% flow statepoint and held constant throughout the perturbed conditions analysis.

As noted in the response to Question 7, core pressure, core inlet subcooling, and perturbed power level are iteration variables in the perturbed conditions analysis.

Core performance during the LFWH analysis is modeled so as to parallel expected plant performance after a 100°F loss of feedwater heating. Best-estimate approximations of system variables are included in the SIMULATE-E analysis. Uncertainties are accounted for by the conservative feedwater temperature reduction used in the analysis. The high simulated thermal power trip, which would mitigate the consequences of this event, is also assumed to be disabled. Thus, the final perturbed power for the analysis is allowed to reach a level which the system would be protected from by this trip.

**NRC Question:**

9. What are the differences between the GSU and vendor methodologies and assumptions for analyzing the LFWH event and the CRWE event?

**GSU Response:**

Analytical conditions and assumptions for both the LFWH and CRWE analyses were based on fuel vendor methodology. The primary differences between fuel vendor and GSU methodologies are the computer programs used in the analysis and the core exposure assumptions.

*CRWE Analysis.* GSU used control rod patterns recommended by the fuel vendor to perform controlled depletion analyses and calculate the hot excess reactivity at the end of each burn increment. The fuel vendor calculated hot excess reactivity through the use of a reverse Haling depletion. Because conditions were taken from the operating cycle benchmarks, the GSU calculations were based on actual end of previous cycle conditions, while the fuel vendor analyses were based on end of cycle exposure conditions predicted several months before the actual end of operation. Design basis calculations performed by GSU for reload support will be based on projected end of cycle conditions.

*LFWH Analysis.* The representative LFWH analysis was performed on the basis of fuel vendor methodology in effect at the time of the Cycle 2 analysis of record.

Prior to the analysis of Cycle 3, the fuel vendor methodology kept core flow rate constant as the feedwater temperature decreased; this method was used for GSU analysis of RBS Cycles 2 and 3. For Cycle 3 conditions, the fuel vendor methodology allowed core flow rate to increase as the fluid temperature decreased.

Because core conditions were taken from operating cycle benchmarks, the GSU calculations were based on actual end of previous cycle conditions, while fuel vendor analyses were based on end of cycle exposure conditions predicted several months before the actual end of operation. Design basis calculations performed by GSU for reload support would typically be based on projected end of cycle conditions.

**NRC Question:**

10. Do the conditions assumed in the analysis of the SLCS cold shutdown margin and the CRWE and LFWH events conservatively bound the expected operating statepoints?

**GSU Response:**

All of the static and quasi-static analyses using SIMULATE-E to support the plant design basis are performed by using a stepwise analysis throughout the cycle to determine the cycle exposure point with the most severe consequences. For the SLCS cold shutdown margin calculation, the point of maximum cold excess reactivity is used; for the CRWE analysis, the point of maximum hot excess reactivity is used. For the LFWH analysis, event consequences determine the most adverse cycle exposure point.

*SLCS Cold Shutdown Margin.* The analysis for the Standby Liquid Control System is performed at cold (68°F), xenon-free conditions with all rods out at the cycle exposure with the highest cold excess reactivity. Consistent with the plant Technical Specifications, the final boron concentration attained by the system is assumed to be 660 ppm, which is substantially lower than the design specification (and expected system performance) of 825 ppm. The SIMULATE-E model is set up with a conservative value of liquid boron cross section. These assumptions conservatively bound expected core operating conditions at cold conditions. Lower shutdown margins at higher temperatures as described by PECO<sup>1</sup> are accounted for in the determination of minimum shutdown margin requirements.

*CRWE Analysis.* The CRWE calculations undertaken as design basis analyses for a reload core are used to verify the applicability of the existing MCPR<sub>p</sub> curves in the Technical Specifications. These curves were established by a generic statistical analysis of CRWE events performed by the NSSS supplier as part of the primary qualification of

---

<sup>1</sup>S.R. Hesse, "Methods for Performing BWR Steady-State Reactor Physics Analysis," PECO-FMS-0005-A, Volume 1, Philadelphia Electric Company (1988).

their BWR/6 product line. Statepoints are selected within the expected operating domain for representative thermal margin analysis. Calculated  $\Delta$ CPR values which result in power-dependent OLMCPR values falling below the generic curve support continued use of the existing limits.

As noted in the response to Question 5, initial conditions for each individual CRWE calculation require the assumption of an unlikely core configuration. The Rod Worth Limiter system prevents the implementation of a configuration which includes a high-worth control rod, so its provisions are ignored in the determination of a limiting control rod pattern. The pattern is further skewed conservatively by the choice of an unrealistically conservative control rod pattern which places a high worth bundle (*i.e.*, one close to the LHGR, MAPLHGR and MCPR operating limits) near a high worth control rod. Additional conservatism is introduced by assuming failure of the operational rod block, which stops control rod movement after two feet of withdrawal, and by assuming erroneous withdrawal of the strongest four-rod gang, although RBS does not currently use ganged rod withdrawal.

*LFWH Analysis.* The representative analyses of the RBS LFWH transient reported in Chapter 7 and in the response to Question 6 were performed at end of cycle conditions. In a reload application, detailed analyses are performed at enough exposure points to determine the most severe statepoint for determination of thermal margin requirements. This requirement may be met through the establishment of a cycle exposure allowance applied to analysis at end of cycle conditions. Conservatism is introduced into the analysis through use of 102% power for definition of the base critical eigenvalue and assumed failure of the simulated thermal power monitor scram, which would normally terminate the event prior to core stabilization at the elevated power. The SIMULATE-E analysis is otherwise best estimate.

**NRC Question:**

11. Discuss the applicability of the vendor analyses of the fuel loading error event to the present and future RBS core reloads.

**GSU Response:**

The accidental misloading of the reactor core may result in degradation of thermal margins if low- and high-reactivity bundles are exchanged in the core arrangement and the reactor is operated at power without correcting the misloading or revising the planned control rod patterns to accommodate the power redistribution. Multiple overchecks during core loading and online core monitoring generally reduce the probability of such operation to very low levels. Because even multiple lines of defense occasionally allow a low-probability event to occur, however, GE has provided a set of generic analyses quantifying the effects of a postulated fuel misloading event.

The analysis of a postulated fuel misloading error consists of selecting a core statepoint and repetitively exchanging bundles until a maximum change in MCPR is established. Although the 624 bundles in the RBS core define a prohibitively large number of cases, most of these permutations can be discarded through symmetry and relative power arguments. For the RBS Control Cell Core, the limiting mislocation event can reasonably be expected to involve the placement of a highly reactive fuel bundle into an active Control Cell. Typical operation in eighth-core symmetry involves seven full or partial control cells and twenty or fewer highly reactive bundles.

In their generic reload qualification<sup>1</sup>, GE demonstrated the basic compliance of their standard fuel designs with a representative analysis. In this generic analysis, the NSSS supplier determined the thermal margin effects of all possible fuel bundle mislocation errors in 16 separate BWR reload core designs, of which two were Control Cell Cores

---

<sup>1</sup>General Electric Company, "GESTAR II," NEDE-24011-P-A-10, p. 1-11 (GE proprietary).

typical of the RBS core loading strategy<sup>1</sup>. This analysis was extended to three BWR/6 reload strategies in a later analysis<sup>2</sup>. Reload fuel design changes are evaluated against this generic analysis through a comparison of critical power effects as predicted by the GEXL-PLUS critical power correlation. Use of standard GE fuel designs is covered by their analysis because the physical effects are not changed by the core analysis methodology. Use of the GE analyses remain appropriate as long as the core is loaded exclusively with GE-fabricated fuel of designs falling within the limits of the generic analysis.

If the RBS core is reloaded with fuel of a design falling outside the limits of the generic analysis (such as would be obtained from a different fuel vendor), methods for analysis of fuel loading errors will be developed internally and a cycle-specific analysis will be provided for the design basis unless the vendor has an applicable generic analysis or provides cycle-specific analysis for the reload.

---

<sup>1</sup>Letter, R.E. Engel (GE) to T.A. Ippolito (NRC), "Change in General Electric Methods for Analysis of Mislocated Bundle Accident," dated November 4, 1980.

<sup>2</sup>Letter, R.E. Engel (GE) to D.B. Vassallo (NRC), "Change in General Electric Methods for Analysis of Mislocated Bundle Accident," dated March 23, 1982.

**NRC Question:**

12. Discuss the nonconservative GSU overprediction (relative to the vendor) of the SLCS cold shutdown margin for the RBS Cycle-3.

**GSU Response:**

The difference between GSU-calculated shutdown margins and the fuel vendor's results are primarily a result of differences in conservatism included in the boron worth modeling assumptions.

SIMULATE-E uses an effective group two boron cross section to model the soluble boron for the SLCS shutdown margin calculation. The boron cross section is obtained from CASMO lattice analyses for specific fuel loaded in the reactor. The effective boron cross section is established conservatively by selecting its lowest value obtained over the cycle exposure range for each lattice type in the core. The choice of the cycle exposure range by lattice type is a reasonable and acceptable range to use in choosing the boron cross section since it bounds the calculation for a specific cycle.

The original Cycle 3 SLCS shutdown margin of 4.2% (reported in Chapter 6) was based on the predicted cold critical eigenvalue. As shown in Table F-6.1 (see response to Question 6), the actual cold critical eigenvalue at BOC3 gave a SLCS cold shutdown margin of 4.4%, verifying that the original reported value is conservative. In the Cycle 1 analysis, the fuel vendor conservatively assumed the borated eigenvalue to be equal to the All Rods In (ARI) eigenvalue. For Cycles 2 and 3, the fuel vendor calculated the 660 ppm borated eigenvalue by subtracting 0.01 from the 600 ppm borated eigenvalue. GSU calculations show the difference between the 660 ppm and 600 ppm borated eigenvalues to be 0.012, confirming the fuel vendor's assumption as conservative.

Since GSU and fuel vendor conservatisms, assumptions, and methodologies are different, the analyses are expected to have different results. Both methods can conservatively verify that the SLCS system can shut down the reactor under all expected core conditions.

**NRC Question:**

13. Have any adjustments been made (e.g., to the albedos or thermal leakage factors) to improve the agreement between the GSU predictions and the benchmark measurements? If so, how do these adjustments affect the inferred calculational uncertainty? Have any benchmark measurements been deleted? If so, please discuss.

**GSU Response:**

A number of adjustment factors are available in SIMULATE-E to normalize calculated results with measured data. Horizontal and vertical albedos, thermal leakage adjustment factors, control rod strength adjustment factors, bypass voiding factors, and partial fuel factors (also termed  $xk$  factors) are all available.

*Albedos.* Horizontal and vertical albedos were calculated in detail for all three of the initial cores included in the benchmarks using the modified ABLE code, however as described in the responses to Questions 1 and 2 the albedos were set equal to those of Cycle 1 and kept constant throughout the 3 cycles. For the Peach Bottom benchmark, detailed second cycle albedos were also calculated and used in the analysis. For the RBS and Quad Cities benchmarks, the same horizontal and vertical albedo factors were retained for all analyzed cycles. None of the albedo factors were adjusted to improve agreement between prediction and measurement, nor have any follow-on cycles been reevaluated for albedos beyond the Peach Bottom analysis. Quad Cities cold calculations used cold conditions albedos taken from the RBS model.

*Thermal Leakage Adjustment.* The thermal leakage adjustment factors were set to values determined in preliminary perturbation analysis and from SIMULATE-E calculations performed by others. The adjustment factors were kept constant throughout all the benchmark analyses.

*Control Rod Strength Adjustment.* A representative set of control rod strength adjustment factors was developed as part of the initial core modeling effort for RBS. These factors were determined by power shapes observed during the first three cycles of operation.

The agreement between incore instrument measurements and SIMULATE-E predictions is observed to be reasonable and acceptable without requiring further manipulation of these factors. Should a systematic degradation of predictive accuracy in the vicinity of inserted control rods be observed, however, these factors would be adjusted consistent with those observations. Use of the control rod strength adjustment factors to account for channel bulging in the Quad Cities analysis was described in the text. Control rod strength adjustment factors were not used in the Peach Bottom benchmark.

*Bypass Voiding.* As noted in section 5.2, SIMULATE-E bypass voiding was required for modeling of the first cycle of Peach Bottom 2. Correlation factors within the bypass void model are used to normalize the calculated results with measurements. Because the RBS core and fuel design maintain sufficient bypass flow to avoid boiling in the bypass region, the bypass void model is not used in RBS analysis.

*Partial Fuel Factors.* These factors are included in the SIMULATE-E coding primarily for use in PWR analysis. They are not used in RBS calculations.

*Excluded Benchmarks.* As noted in the text, a number of statepoint predictions have been excluded from the determination of uncertainties for application of the SIMULATE-E model to RBS design basis analyses. In the Quad Cities gamma scan benchmarks, the peripherally loaded mixed oxide fuel bundle was excluded from the local power distribution benchmark evaluation because its location induced azimuthal power gradients which were beyond the capability of CASMO to predict. In both the Quad Cities and Peach Bottom TIP benchmarks, the difference in plant configuration and power density led to exclusion of all predictions from the determination of RBS TIP uncertainty.

In the RBS eigenvalue uncertainty analysis, a number of statepoints were excluded from the evaluation because of neutronic effects which were not within the capability of the SIMULATE-E modeling. RBS benchmarks were taken from the core follow analysis, which in some instances modeled an exposure increment with a representative core configuration to avoid frequent data changes. These approximations were most inaccurate at beginning of life because most of the exposure before 1000 MWd/T was accumulated in small increments not explicitly modeled in the analysis. Early in the first operating cycle, several predicted statepoints were excluded because of extensive power changes during startup testing; these changes brought about core variations which induced

fission product transients that did not equilibrate to predictable levels until approximately 600 MWd/T cycle exposure. Further adjustments to the RBS cold critical eigenvalue database are described in the response to Question 4.

**NRC Question:**

14. What is causing the systematic increase in the RBS Cycles 2 and 3 hot and cold critical eigenvalues with exposure?

**GSU Response:**

The behavior of cold critical eigenvalue predictions over the first three RBS operating cycles is discussed in the response to Question 4. In that response, cycle exposure effects were not addressed because the valid reload benchmark statepoints occur at beginning of cycle conditions. The remainder of this response addresses the exposure-dependent increase in the hot critical eigenvalue; exposure-dependent cold eigenvalue effects are similar to those discussed below.

The GSU calculated eigenvalues exhibit a steady increase as core exposure is accumulated. This increase is mild and predictable, and its origins are generally attributed to the treatment of burnable absorber material in the lattice physics analysis.

Industry experience with MICBURN is characterized by a general underprediction of the depletion of gadolinia burnable absorber with increasing exposure. For any given nodal exposure, a gadolinia-loaded fuel bundle will contain more gadolinia than the MICBURN-defined model. The GSU modeling allowed for this MICBURN shortcoming by increasing the dimensions of the burnable absorber fuel rod water region. This adjustment, which increased the neutron thermalization and the burnable absorber depletion rate, performed well for the initial cycle but resulted in an overprediction of gadolinia depletion for subsequent cycles. Since the existing methods result in mild and predictable errors, changes in methodology are unnecessary.

The relative worth of burnable absorber in the RBS core is shown in Figure F-14.1. The parameter plotted against the y-axis is the total reactivity contained in unburned gadolinia in the core as calculated by SIMULATE-E from CASMO estimates of exposure-dependent burnable absorber worth for each lattice type. Because of its lower gadolinia loading, the Cycle 1 curve is shallower than the subsequent cycles. The figure shows

a faster burnable absorber depletion rate for Cycle 2, which also shows the greatest eigenvalue slope over the cycle.

Critical eigenvalue trends during depletion are shown as a function of gadolinia reactivity worth in Figure F-14.2. While the Cycle 1 data are relatively constant, both of the reload cycles show increasing eigenvalues as the gadolinia is depleted. These trends indicate that the higher level of burnable absorber loading in the reload cycles results in a greater overprediction of gadolinia depletion for these cycles.

Figure F-14.1  
Gadolinia Worth vs Cycle Exposure  
RBS Cycles 1-3

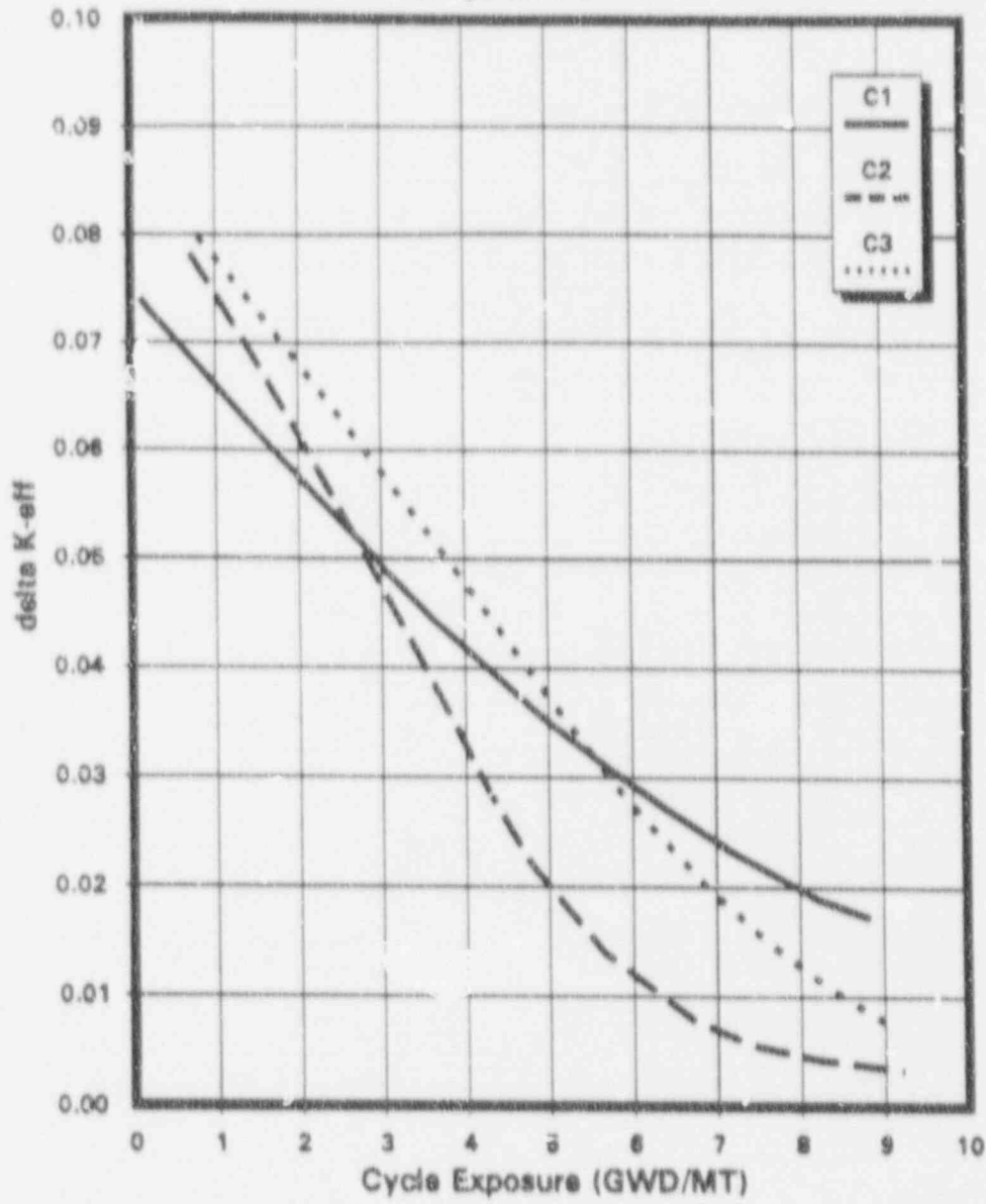
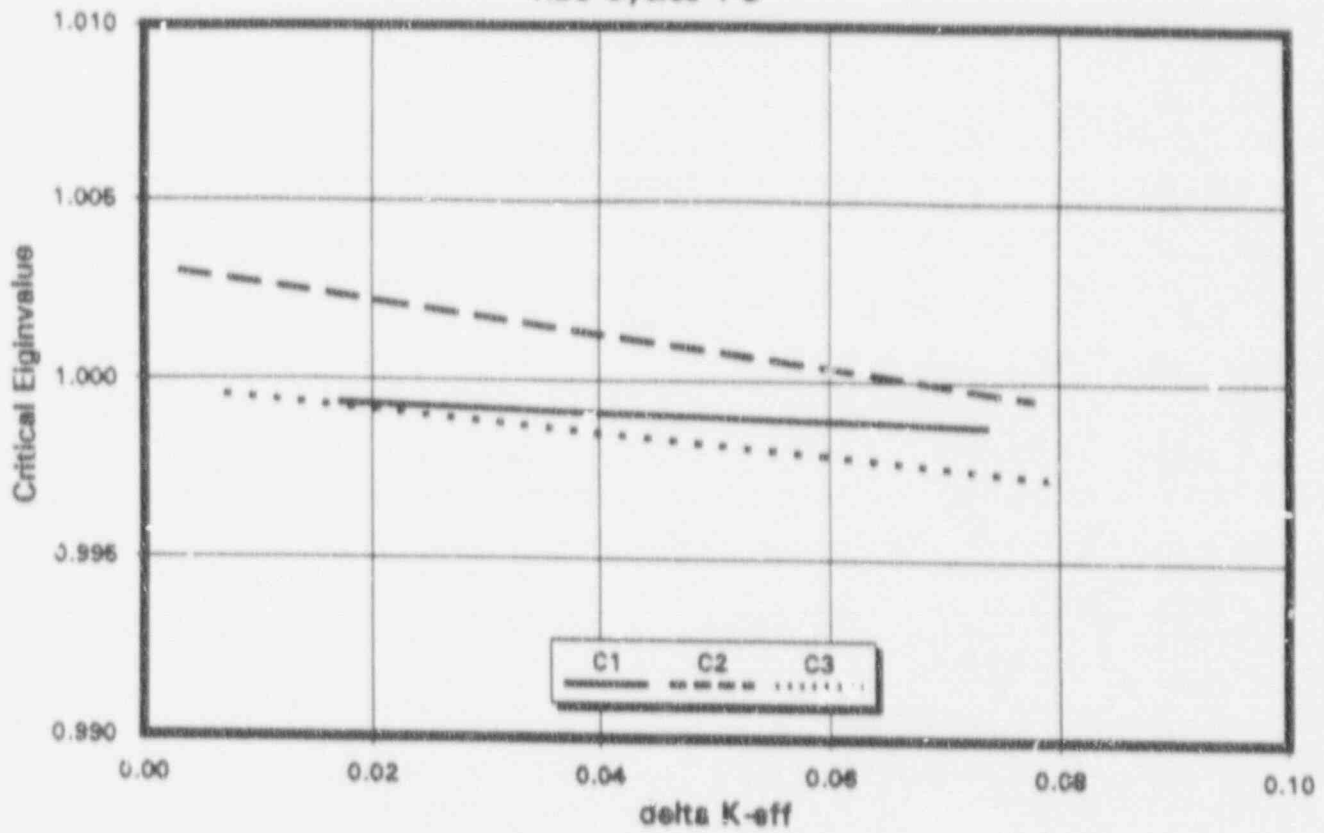


Figure F-14.2  
Critical Eigenvalue vs Gadolinia Worth  
RBS Cycles 1-3



**NRC Question:**

15. Have any SIMULATE-E comparisons been made to local cold critical measurements? If so, how do the results compare to the in-sequence criticals?

**GSU Response:**

SIMULATE-E predictions of local critical data from Quad Cities Unit 1 have been reported by others<sup>1</sup>. These analyses showed that SIMULATE-E predicted local criticality with similar consistency and accuracy to that observed in the prediction of in-sequence criticals.

The Quad Cities model used in the Appendix A benchmarks was exercised to predict the critical eigenvalue in a number of local cold critical measurements not present in the EPRI data. Data for these analyses were provided by the Quad Cities licensee.

Post-submittal re-evaluation of Quad Cities SIMULATE-E cold model results presented in Appendix A identified a means to improve upon previous cold model results. This improvement arises from eliminating use of control rod strength adjustment factors in SIMULATE-E modeling of Quad Cities lattice types under cold conditions. The in-sequence critical benchmarks described in Appendix A have been re-analyzed with the revised cold model. Local critical benchmarks have been also been analyzed with the revised cold model.

The results of both critical analyses are summarized in Table 15.1. Quad Cities in-sequence critical benchmarking now results in a mean cold critical eigenvalue of 0.99812 with a standard deviation of 0.0027 as compared to results presented in Appendix A, Table A-5. The mean cold critical eigenvalue for all Quad Cities criticals presented in

---

<sup>1</sup>A. Dyszel, K.C. Knoll, J.H. Emmett, E.R. Jebson, C.R. Lehmann, A.J. Roscioli, R.M. Rose, J.P. Spadaro, and W.J. Weadon, "Qualification of Steady State Core Physics Methods for BWR Design and Analysis," PL-NF-87-001-A, Pennsylvania Power & Light Company (1987).

Table 15.1 is 0.99600 with a standard deviation of 0.0023. These results indicate good overall agreement between local and in-sequence critical benchmarking results.

Table F-15.1  
Summary of Quad Cities Critical Predictions

Exposure	SIMULATE-E k-effective	Period Correction	Critical Eigenvalue
0.000 <sup>1</sup>	1.00140	0.00035	1.00105
0.000	0.99738	0.00103	0.99635
2.864 <sup>1</sup>	0.99584	0.00025	0.99559
3.748 <sup>1</sup>	0.99690	0.00025	0.99665
3.748	0.99695	0.00070	0.99625
3.748	0.99727	0.00105	0.99622
3.748	0.99786	0.00129	0.99657
3.748	0.99772	0.00120	0.99652
3.748	0.99562	0.00029	0.99533
3.748	0.99689	0.00101	0.99588
3.748	0.99527	0.00021	0.99506
3.748	0.99660	0.00110	0.99550
3.748	0.99541	0.00046	0.99495
3.748	0.99558	0.00052	0.99506
3.748	0.99338	0.00046	0.99292
3.748	0.99289	0.00070	0.99219
3.748	0.99460	0.00024	0.99436
3.748	0.99416	0.00034	0.99382
3.748	0.99242	0.00027	0.99215
4.946 <sup>1</sup>	0.99574	0.00115	0.99459
6.922 <sup>1</sup>	0.99791	0.00024	0.99767
7.835 <sup>1</sup>	0.99760	0.00060	0.99700
8.698 <sup>1</sup>	1.00299	0.00109	1.00190
10.156 <sup>1</sup>	1.00097	0.00047	1.00050

<sup>1</sup>In-sequence critical; included for comparison

**NRC Question:**

16. Discuss the increasing traversing incore probe (TIP) asymmetry during Cycles 1, 2 and 3.

**GSU Response:**

The increasing asymmetry in the measured TIP responses over time indicates that the detectors and the mechanisms which move them through the core are aging. As this equipment grows older, the accuracy of its response and performance also deteriorates; the difference in readings between symmetric instrument pairs is an indication of the uncertainty in the readings.

Actual TIP uncertainty is calculated during instrument calibration measurements at the beginning of each operating cycle as an indication of TIP reproducibility and to assure that instrument performance remains within acceptable limits. At the beginning of Cycle 3, the overall TIP uncertainty was found to be 2.83% while the observed asymmetry was 3.05%. At the beginning of Cycle 2, the uncertainty was 2.15% while the observed asymmetry was 2.23%. The first evaluation was performed near the end of Cycle 1 operation and resulted in an overall TIP uncertainty of 2.13%, compared with an observed asymmetry of 1.72%. These comparisons show the validity of the observed asymmetry as an indication of measurement uncertainty. Since actual uncertainties are determined at a single statepoint in each cycle, observed asymmetries provide the best inference of instrument errors over the cycle.

Uncertainty in the instrument readings derives from a number of sources. The count rate from the fission chambers themselves is not expected to vary greatly over the lifetime of the detector, but the chamber positioning within the instrument space becomes less certain as the reactor internals accumulate exposure. The radial positioning of the fission chamber at the time of recording is determined by the instrument tube in which the instrument travels. Under irradiation, the instrument tubes may exhibit bowing or swelling, allowing or inducing movement of the fission chamber away from the nominal center of the instrument space and changing the magnitude of the flux seen by the detector.

Axial positioning within the instrument tube is determined by the travel measurement of the TIP machine. As the sensor wire unwinds, the axial position is determined by a revolution counter on the wire spool. Nonuniform stacking of the instrument wire on the spool can change the relationship between revolutions and axial deflection, and the mechanical revolution counter may undergo performance degradation. This effect has a small impact on TIP asymmetry, which is based on axially integrated instrument readings, but it may increase the apparent errors in individual readings by inducing axial positioning error in the measurements.

**NRC Question:**

17. Discuss the applicability of the Quad Cities-1, Peach Bottom-2 and RBS Cycles 1-3 benchmark data in determining the SIMULATE-E calculational uncertainties for the RBS reload cores.

**GSU Response:**

This technical report demonstrates the capabilities of the GSU engineering staff to formulate and execute design analyses for BWR plants. The primary purpose of the benchmarks presented in Appendices A-C is to demonstrate these capabilities and to quantify the accuracy of the methodologies used in the analysis.

As demonstration of the intended application, the RBS analyses are the most appropriate modeling benchmarks. Depletion analysis through three operating cycles with consistent accuracy in predicting incore instrument responses shows the adequacy of the methods and models and demonstrates staff capabilities in modeling the full spectrum of normal operating conditions.

Although the reactor is physically different from the RBS application, the Quad Cities benchmarks provide a quantitative assessment of the analytical models in predicting smaller scale phenomena than are available in the RBS data. The Quad Cities data were chosen because of the gamma scan data for both once- and twice-irradiated fuel, which are not readily available for platforms more similar to RBS.

The Peach Bottom analyses were undertaken in support of RETRAN benchmarking of the turbine trip tests performed at the end of Cycle 2. The TIP benchmarks provided a direct indication of the adequacy of the model in predicting power distribution within the core and allowed an immediate measure of the validity of the data passed to RETRAN. Both the Quad Cities and Peach Bottom TIP benchmark data, however, exhibited asymmetry errors substantially greater than the RBS TIP benchmark data. These high asymmetry errors indicate confidence in the measured Quad Cities and Peach Bottom TIP data for benchmarking purposes is much lower than for RBS data. Only RBS TIP data were used in determining the RBS TIP uncertainty.

**NRC Question:**

18. Are the RBS moveable detectors  $\gamma$ -TIPs? If so, discuss the use of the Quad Cities-1 and Peach Bottom-2 benchmark data in determining the SIMULATE-E calculational uncertainties for the RBS reload cores.

**GSU Response:**

As was the case with the EPRI-published benchmark data, the TIP instruments within the RBS core are fission chambers. They provide the same general response and have some of the same uncertainty factors as the instruments in the older plants. Evolving BWR system design has provided the RBS instruments with greater reliability, as is evidenced by the lower TIP prediction errors for the RBS analyses than for either the Peach Bottom or the Quad Cities analyses.

The primary design difference between the RBS detector system and the one in use at Peach Bottom and Quad Cities is the geometry of the instrument tubes. Configured for the narrow-narrow gap in a D-lattice arrangement, the older instrument tube design held the TIP tube physically closer to one of the surrounding bundles than to the other three. In the RBS configuration, the TIP tube is located at the center of the instrument tube, equidistant from the four adjacent bundles. This arrangement facilitates the arithmetic combination of contributions from these four bundles and reduces the uncertainty associated with azimuthal position within the gap.

The benchmark TIP predictions from Quad Cities and Peach Bottom were not used in determining the RBS TIP uncertainty. As noted in Chapter 6, the level of uncertainty in plant operating conditions leading up to TIP dataset collection made these applications substantially less reliable than the RBS data for determination of TIP error.

**NRC Question:**

19. Justify the conclusion that the equilibration of the process variables during the CRWE event results in a conservative  $\Delta$ CPR calculation.

**GSU Response:**

MCPR is primarily a function of bundle power and bundle flow rate. As bundle power is increased, the calculation is also affected by a second-order interaction between power and flow: as power increases, two-phase pressure drop also increases and total flow is decreased. If the process variables are allowed to equilibrate during the CRWE transient analysis, the flow through the bundles around the error rod will decrease as the power rises. Because the event progresses more rapidly than the flow can respond, this flow decrease is not realized in the physical event until after the transient is terminated by a reactor scram. In the analytical model, the flow decrease causes a higher, more conservative value of  $\Delta$ CPR.

**NRC Question:**

20. Has the worst-case combination of LPRM detector and channel failures been assumed in the determination of the rod block monitor response during the CRWE event?

**GSU Response:**

The failure of individual instruments was not considered in the CRWE analysis. As was the case with the other applications analyses, the CRWE calculation was included to demonstrate GSU staff capabilities in modeling events of this type.

RBS uses the Rod Withdrawal Limiter (RWL) to minimize the effects of erroneous control rod withdrawal. The RWL is a two-channel subsystem of the Rod Control and Information System (RC&IS), which facilitates incore management of the control rods. The RWL mitigates the consequences of the CRWE event by limiting the continuous movement of a selected control rod or gang to 24 inches at medium power and 12 inches at high power. For the RWL, high power is defined by the High Power Setpoint and medium power is defined by the Low Power Setpoint. Below the Low Power Setpoint, the RWL does not function; rather, control rod movements are restricted by the Banked Position Withdrawal Sequence as enforced by the Rod Pattern Controller (RPC) subsystem of RC&IS. Both RWL and RPC enforce control rod movement restrictions on the basis of rod position switches. Neither of these subsystems is dependent on the readings of incore instruments, so combinations of individual detector failures and channel failures were not considered.

The rod block noted in the results of the CRWE analysis is the flow-biased rod block function, which is based on the APRM estimate of core power. While the APRM system depends on readings from individual LPRM instruments, these readings are averaged to determine core average power and are limited by the Technical Specifications in the number of inoperative instruments allowed in each of the channels.

**NRC Question:**

21. Discuss the assumption that the observed TIP asymmetry is a measurement error rather than a real physical power tilt. If the TIP asymmetry is considered to be the result of an actual power asymmetry, how will this affect the inferred RBS TIP uncertainty?

**GSU Response:**

Asymmetry in the RBS TIP measurements is not likely to be the result of actual power tilts. The tabulated individual asymmetry factors show both positive and negative values, indicating that neither half of the core was consistently higher than the other in its measured TIPs. Actual power differences would also be evident in imbalances in the LPRM readings.

As noted in the response to Question 16, the measurement of TIP uncertainties at the beginning of each operating cycle has shown a close agreement between measured uncertainty and the uncertainty inferred from asymmetry in the TIP integrals.

If the observed TIP asymmetry is a result of azimuthal power gradients rather than measurement error within the instrumentation, then no reduction in the TIP error can be inferred from the asymmetry. Under these conditions, the TIP prediction error is equal to the raw error value reported in Chapter 6, or 7.6% over three cycles. In the determination of overall RBS TIP prediction error, the use of TIP asymmetry as an indication of measurement error reduces the TIP prediction error by 0.5%.

A more serious impact of the assumption that TIP asymmetry is an indication of actual power tilts is the concurrent observation that the SIMULATE-E model predicts perfect symmetry in all of these conditions. In the RBS analysis, where all of the depletion steps were executed in quarter and eighth-core symmetry, the analytical symmetry is imposed by the configuration assumed in the analysis. Actual power tilts in the RBS core would degrade the accuracy of the symmetrical core model and would require the use of full-core calculations for core follow and core design analysis.

In the Quad Cities analysis, which was physically asymmetrical and required full core analysis, near perfect analytical symmetry was also noted in most of the TIP predictions. In the Quad Cities analysis, as in the RBS analysis, SIMULATE-E did not predict power tilts of magnitudes similar to the observed TIP asymmetry. Results of the gamma scan benchmarks reported in Appendix A indicate that the SIMULATE-E model predicted core power distributions correctly and did not miss any significant azimuthal gradients within the core. The Quad Cities benchmark indicates that SIMULATE-E adequately represents major core phenomena to the point that nodal power distributions are consistent with measured data.

**ATTACHMENT 2**

**Errata Pages to be Replaced**

PHYSICS TOPICAL REPORT

EA-CA-0601-M

January 31, 1991

Revision 0 Errata

<u>NUM</u>	<u>LOCATION</u>	<u>PROBLEM DESCRIPTION</u>
1	Cover	Add Lynn A. Leatherwood to CONTRIBUTORS
2	Page 48	Include square root sign in formula for uncertainty.
3	p 58- 59	Change: The calculated target k-effective rms... to read: The target minus calculated k-effective rms... Averages are not in proper columns.
4	Table 6.12	8.0 REFERENCES needs to be left justified.
5	Page 118	Change scale on Y-axis.
6	Figure 7.6	Align start of description to align with descriptions on pp 128-131.
7	pp 124-128	Align in the same manner as pp 128-131.
8	pp 277-279	CAVEX values for CY02 & CY03 are CYCLEX in GWD/st. Change to CAVEX in GWD/mt. Cycle 1 is in GWD/mt as it should be.
9	Table C-3	

STEADY STATE CORE PHYSICS METHODS  
FOR BWR DESIGN AND ANALYSIS

January 1991

Principal Engineer

Mr. H. Greene

Contributors

Dennis C. Albright  
Brian J. Boyle  
Jon Juneau  
Lynn A. Leatherwood  
Gary W. Scronce  
Phu Van Vo

Review:

Lynn A. Leatherwood

L.A. Leatherwood  
Supervisor - Core Analysis

1/30/91

Date

Approve:

J. S. Miller

J.S. Miller  
Director - Engineering Analysis

1/30/91

Date

Gulf States Utilities Company  
River Bend Station  
P.O. Box 220  
St. Francisville, Louisiana 70775

~~9100070433~~ 1677

$$\sigma = \sqrt{\frac{\sum (V_i - V_m)^2}{N-1}}$$

where  $\sigma$  is the standard deviation and  $V_m$ ,  $V_i$ , and  $N$  are as defined above.

### 6.1 RADIAL POWER UNCERTAINTY

Predictions of RBS TIP data were used to calculate the uncertainty in the radial power distribution. The individual TIP readings were integrated over each active string to provide an indication of the radial power distribution. The predicted and measured radial TIP distributions were normalized over the core. The normalized predictions were compared with normalized measurements and a radial power uncertainty factor was determined. This uncertainty factor represents a four-bundle radial power distribution because of the incore instrument configuration; comparison of this result with the radial power result of the Quad Cities gamma scan benchmark provides an overall radial power uncertainty factor.

reactivity for River Bend Cycle 3. The total k-effective sensitivity due to measurement uncertainties is 0.00171  $\Delta k$ . SIMULATE-E calculations of hot critical core k-effective for the data points in the benchmark result in an rms difference which is less than this uncertainty.

#### 6.4.2 Prediction of Cold Critical Eigenvalue

Cold eigenvalues (k-effective) were calculated with SIMULATE-E for 27 critical statepoints from three cycles of RBS operation. The critical statepoints were xenon-free core conditions at moderator temperatures ranging from 100°F to 500°F. Cold critical eigenvalues for other core conditions were computed but not included in the cold critical evaluation. These criticals would have introduced uncertainty factors which are not directly relevant to the determination of a mean cold eigenvalue for the RBS SIMULATE-E model.

Table 6.10 contains results of the River Bend Station cold criticals. The core critical k-effective in Table 6.10 includes a reactor period correction which is typically less than 0.001. The target minus calculated

k-effective rms difference is 0.322% for the three RBS cycles.

Figure 6.1 shows the cold results together with those of the hot benchmark. The bias between hot and cold target k-effective is constant and does not exhibit exposure or gadolinia dependencies. This constant bias allows the determination of cold target k-effective from hot critical calculations.

#### 6.5 TIP UNCERTAINTY

The River Bend, the Quad Cities and the Peach Bottom TIP predictions were evaluated for asymmetry about the TIP symmetry axis. Both the Quad Cities/Peach Bottom TIP benchmarks showed substantial asymmetric errors. Since the observed errors were substantially greater than those of the River Bend TIP measurements, the Quad Cities and the Peach Bottom TIP predictions were not included in the determination of an overall GSU calculated TIP uncertainty.

The River Bend TIP evaluation was performed by tabulating the difference between nominally symmetric TIP integrals and generating an rms error value for each TIP

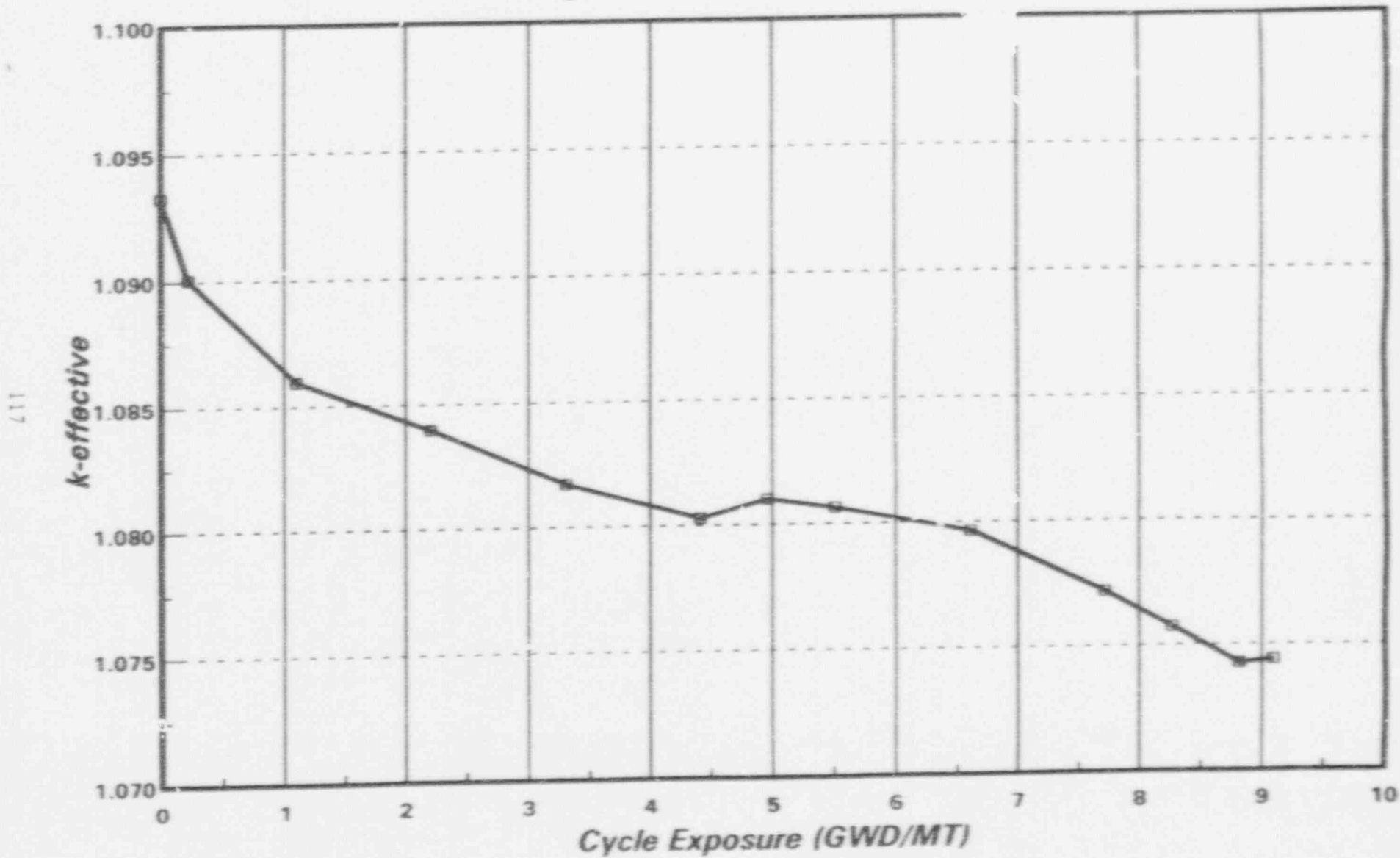
Table 6.12  
RBS TIP Uncertainty

<u>Statepoint Date</u>	<u>RMS Error in Ind. Readings</u>	<u>Inferred TIP Uncertainty</u>
05/26/86	6.0%	5.8%
06/19/86	6.5%	6.2%
07/26/86	5.8%	5.6%
08/27/86	7.4%	7.2%
09/17/86	6.7%	6.5%
12/31/86	11.5%	11.3%
01/28/87	7.4%	7.2%
02/15/87	7.2%	7.0%
03/24/87	6.8%	6.6%
04/27/87	6.3%	6.0%
05/14/87	7.3%	7.0%
06/16/87	3.2%	2.5%
06/30/87	8.0%	7.7%
07/29/87	8.6%	8.4%
09 - /87	10.9%	10.8%
<b>Cycle 1 Average</b>	<b>7.6%</b>	<b>7.3%</b>
01/22/88	6.9%	6.5%
02/17/88	3.8%	2.6%
03/23/88	11.1%	10.9%
04/29/88	11.4%	11.2%
07/22/88	3.4%	2.7%
08/24/88	6.2%	5.9%
09/28/88	6.0%	5.7%
10/26/88	5.9%	5.6%
01/26/89	10.1%	9.8%
<b>Cycle 2 Average</b>	<b>7.7%</b>	<b>7.4%</b>
07/17/89	3.4%	1.5%
10/24/89	4.6%	1.1%
03/15/90	8.2%	7.4%
04/16/90	8.3%	7.1%
05/15/90	9.3%	8.8%
06/04/90	7.4%	6.1%
07/02/90	6.6%	5.3%
08/08/90	9.5%	8.7%
<b>Cycle 3 Average</b>	<b>7.4%</b>	<b>6.4%</b>
<b>Three-Cycle Average</b>		<b>7.1%</b>

8.0 REFERENCES

1. D.M. Ver Planck, W.R. Cobb, R.S. Borland, and P.L. Versteegen, "SIMULATE-E: A Nodal Core Analysis Program for Light Water Reactors; Computer Code User's Manual," EPRI NP-2792-CCM, Electric Power Research Institute (1983).
2. B.M. Rothleder, "EPRI-NODE-P," Advanced Recycle Methodology Program System Documentation, EPRI Research Project 118-1, Part II, Chapter 14, Electric Power Research Institute (1977).
3. E.D. Kendrick, Jr., and J.R. Fisher, "EPRI-NODE-B," Advanced Recycle Methodology Program System Documentation, EPRI Research Project 118-1, Part II, Chapter 15, Electric Power Research Institute (1977).
4. D.L. Delp, D.L. Fischer, J.M. Harrison, and M.J. Stedwell, "FLARE, A Three-Dimensional Boiling Water Reactor Simulator," GEAP-4589, General Electric Company (1968).
5. A. Ancona, "Reactor Nodal Methods Using Response Matrix Techniques," Ph.D. Thesis, Rensselaer Polytechnic Institute (December 1977).
6. K.S. Smith, "Assembly Homogenizing Techniques for Light Water Reactor Analysis," *Progress in Nuclear Energy*, Vol. 17, No. 3 (1986), p. 303-335.
7. W.R. Cadwell, "PDQ-7 Reference Manual," WPD-TH678, Westinghouse Electric Corporation (1967).
8. "GEXL-Plus Correlation Application to BWR/2-6 Reactors, GE6 Through GE8 Fuel, NEDC-31598P, General Electric Company (1988); proprietary.
9. B.J. Gitnick, R.R. Gay, R.S. Borland, and A.F. Ansari, "FIBWR: A Steady-State Core Flow Distribution Code for Boiling Water Reactors;

Figure 7.6  
Determination of Most Reactive Exposure Point  
For RBS Cycle 3 SLCS Effectiveness Analysis



## LIST OF FIGURES

A-1	Quad Cities Unit 1 Core Configuration . . .	142
A-2	Quad Cities Unit 1 Critical Eigenvalue Calculated by SIMULATE-E . . . . .	143
A-3	TIP Predictions vs Measurements, Quad Cities 1 Cycle 2, June 29, 1972 . . . . .	144
A-4	Predicted vs Measured TIP Integrals, Quad Cities 1 Cycle 1, June 29, 1972 . . . . .	145
A-5	TIP Predictions vs Measurements, Quad Cities 1 Cycle 1, August 30, 1972 . . . . .	146
A-6	Predicted vs Measured TIP Integrals, Quad Cities 1 Cycle 1, August 30, 1972 . . . . .	147
A-7	TIP Predictions vs Measurements, Quad Cities 1 Cycle 1, September 11, 1972 . . . . .	148
A-8	Predicted vs Measured TIP Integrals, Quad Cities 1 Cycle 1, September 11, 1972 . . . . .	149
A-9	TIP Predictions vs Measurements, Quad Cities 1 Cycle 1, November 1, 1972 . . . . .	150
A-10	Predicted vs Measured TIP Integrals, Quad Cities 1 Cycle 1, November 1, 1972 . . . . .	151
A-11	TIP Predictions vs Measurements, Quad Cities 1 Cycle 1, December 26, 1972 . . . . .	152
A-12	Predicted vs Measured TIP Integrals, Quad Cities 1 Cycle 1, December 26, 1972 . . . . .	153
A-13	TIP Predictions vs Measurements, Quad Cities 1 Cycle 1, March 8, 1973 . . . . .	154
A-14	Predicted vs Measured TIP Integrals, Quad Cities 1 Cycle 1, March 8, 1973 . . . . .	155
A-15	TIP Predictions vs Measurements, Quad Cities 1 Cycle 1, May 16, 1973 . . . . .	156
A-16	Predicted vs Measured TIP Integrals, Quad Cities 1 Cycle 1, May 16, 1973 . . . . .	157
A-17	TIP Predictions vs Measurements, Quad Cities 1 Cycle 1, June 6, 1973 . . . . .	158
A-18	Predicted vs Measured TIP Integrals, Quad Cities 1 Cycle 1, June 6, 1973 . . . . .	159
A-19	TIP Predictions vs Measurements, Quad Cities 1 Cycle 1, July 19, 1973 . . . . .	160
A-20	Predicted vs Measured TIP Integrals, Quad Cities 1 Cycle 1, July 19, 1973 . . . . .	161
A-21	TIP Predictions vs Measurements, Quad Cities 1 Cycle 1, August 30, 1973 . . . . .	162
A-22	Predicted vs Measured TIP Integrals, Quad Cities 1 Cycle 1, August 30, 1973 . . . . .	163

A-23	TIP Predictions vs Measurements, Quad Cities 1 Cycle 1, November 1, 1973 . . . . .	164
A-24	Predicted vs Measured TIP Integrals, Quad Cities 1 Cycle 1, November 1, 1973 . . . . .	165
A-25	TIP Predictions vs Measurements, Quad Cities 1 Cycle 1, December . . . . . 1973 . . . . .	166
A-26	Predicted vs Measured TIP Integrals, Quad Cities 1 Cycle 1, December 11, 1973 . . . . .	167
A-27	TIP Predictions vs Measurements, Quad Cities 1 Cycle 1, December 29, 1973 . . . . .	168
A-28	Predicted vs Measured TIP Integrals, Quad Cities 1 Cycle 1, December 29, 1973 . . . . .	169
A-29	TIP Predictions vs Measurements, Quad Cities 1 Cycle 1, February 13, 1974 . . . . .	170
A-30	Predicted vs Measured TIP Integrals, Quad Cities 1 Cycle 1, February 13, 1974 . . . . .	171
A-31	TIP Predictions vs Measurements, Quad Cities 1 Cycle 1, March 5, 1974 . . . . .	172
A-32	Predicted vs Measured TIP Integrals, Quad Cities 1 Cycle 1, March 5, 1974 . . . . .	173
A-33	TIP Predictions vs Measurements, Quad Cities 1 Cycle 1, March 26, 1974 . . . . .	174
A-34	Predicted vs Measured TIP Integrals, Quad Cities 1 Cycle 1, March 26, 1974 . . . . .	175
A-35	TIP Predictions vs Measurements, Quad Cities 1 Cycle 2, July 26, 1974 . . . . .	176
A-36	Predicted vs Measured TIP Integrals, Quad Cities 1 Cycle 2, July 26, 1974 . . . . .	177
A-37	TIP Predictions vs Measurements, Quad Cities 1 Cycle 2, August 15, 1974 . . . . .	178
A-38	Predicted vs Measured TIP Integrals, Quad Cities 1 Cycle 2, August 15, 1974 . . . . .	179
A-39	TIP Predictions vs Measurements, Quad Cities 1 Cycle 2, September 12, 1974 . . . . .	180
A-40	Predicted vs Measured TIP Integrals, Quad Cities 1 Cycle 2, September 12, 1974 . . . . .	181
A-41	TIP Predictions vs Measurements, Quad Cities 1 Cycle 2, October 23, 1974 . . . . .	182
A-42	Predicted vs Measured TIP Integrals, Quad Cities 1 Cycle 2, October 23, 1974 . . . . .	183
A-43	TIP Predictions vs Measurements, Quad Cities 1 Cycle 2, November 18, 1974 . . . . .	184
A-44	Predicted vs Measured TIP Integrals, Quad Cities 1 Cycle 2, November 18, 1974 . . . . .	185
A-45	TIP Predictions vs Measurements, Quad Cities 1 Cycle 2, December 11, 1974 . . . . .	186

A-46	Predicted vs Measured TIP Integrals, Quad Cities 1 Cycle 2, December 11, 1974 . . . . .	187
A-47	TIP Predictions vs Measurements, Quad Cities 1 Cycle 2, April 3, 1975 . . . . .	188
A-48	Predicted vs Measured TIP Integrals, Quad Cities 1 Cycle 2, April 3, 1975 . . . . .	189
A-49	TIP Predictions vs Measurements, Quad Cities 1 Cycle 2, June 19, 1975 . . . . .	190
A-50	Predicted vs Measured TIP Integrals, Quad Cities 1 Cycle 2, June 19, 1975 . . . . .	191
A-51	TIP Predictions vs Measurements, Quad Cities 1 Cycle 2, August 8, 1975 . . . . .	192
A-52	Predicted vs Measured TIP Integrals, Quad Cities 1 Cycle 2, August 8, 1975 . . . . .	193
A-53	TIP Predictions vs Measurements, Quad Cities 1 Cycle 2, October 20, 1975 . . . . .	194
A-54	Predicted vs Measured TIP Integrals, Quad Cities 1 Cycle 2, October 20, 1975 . . . . .	195
A-55	TIP Predictions vs Measurements, Quad Cities 1 Cycle 2, November 13, 1975 . . . . .	196
A-56	Predicted vs Measured TIP Integrals, Quad Cities 1 Cycle 2, November 13, 1975 . . . . .	197
A-57	Predicted vs Measured Radial La <sup>140</sup> Activity at 3" Above Bottom of Active Fuel . . . . .	198
A-58	Predicted vs Measured Radial La <sup>140</sup> Activity at 9" Above Bottom of Active Fuel . . . . .	199
A-59	Predicted vs Measured Radial La <sup>140</sup> Activity at 15" Above Bottom of Active Fuel . . . . .	200
A-60	Predicted vs Measured Radial La <sup>140</sup> Activity at 21" Above Bottom of Active Fuel . . . . .	201
A-61	Predicted vs Measured Radial La <sup>140</sup> Activity at 27" Above Bottom of Active Fuel . . . . .	202
A-62	Predicted vs Measured Radial La <sup>140</sup> Activity at 33" Above Bottom of Active Fuel . . . . .	203
A-63	Predicted vs Measured Radial La <sup>140</sup> Activity at 40" Above Bottom of Active Fuel . . . . .	204
A-64	Predicted vs Measured Radial La <sup>140</sup> Activity at 45" Above Bottom of Active Fuel . . . . .	205
A-65	Predicted vs Measured Radial La <sup>140</sup> Activity at 51" Above Bottom of Active Fuel . . . . .	206
A-66	Predicted vs Measured Radial La <sup>140</sup> Activity at 56" Above Bottom of Active Fuel . . . . .	207
A-67	Predicted vs Measured Radial La <sup>140</sup> Activity at 63" Above Bottom of Active Fuel . . . . .	208

A-68	Predicted vs Measured Radial La <sup>140</sup> Activity at 69" Above Bottom of Active Fuel . . . . .	209
A-69	Predicted vs Measured Radial La <sup>140</sup> Activity at 75" Above Bottom of Active Fuel . . . . .	210
A-70	Predicted vs Measured Radial La <sup>140</sup> Activity at 81" Above Bottom of Active Fuel . . . . .	211
A-71	Predicted vs Measured Radial La <sup>140</sup> Activity at 87" Above Bottom of Active Fuel . . . . .	212
A-72	Predicted vs Measured Radial La <sup>140</sup> Activity at 93" Above Bottom of Active Fuel . . . . .	213
A-73	Predicted vs Measured Radial La <sup>140</sup> Activity at 99" Above Bottom of Active Fuel . . . . .	214
A-74	Predicted vs Measured Radial La <sup>140</sup> Activity at 103" Above Bottom of Active Fuel . . . . .	215
A-75	Predicted vs Measured Radial La <sup>140</sup> Activity at 109" Above Bottom of Active Fuel . . . . .	216
A-76	Predicted vs Measured Radial La <sup>140</sup> Activity at 118" Above Bottom of Active Fuel . . . . .	217
A-77	Predicted vs Measured Radial La <sup>140</sup> Activity at 123" Above Bottom of Active Fuel . . . . .	218
A-78	Predicted vs Measured Radial La <sup>140</sup> Activity at 129" Above Bottom of Active Fuel . . . . .	219
A-79	Predicted vs Measured Radial La <sup>140</sup> Activity at 134" Above Bottom of Active Fuel . . . . .	220
A-80	Predicted vs Measured Radial La <sup>140</sup> Activity at 141" Above Bottom of Active Fuel . . . . .	221
A-81	Discharge Axial Power Distribution vs Measured La <sup>140</sup> Activity for Bundles CX0683, CX0420, CX0440, CX0445, CX0362, and CX0643	222
A-82	Discharge Axial Power Distribution vs Measured La <sup>140</sup> Activity for Bundles CX0384, CX0327, CX0611, CX0631, CX0100, and CX0162	223
A-83	Discharge Axial Power Distribution vs Measured La <sup>140</sup> Activity for Bundles CX0520, CX0052, CX0351, CX0723, GEB105, and CX0397	224
A-84	Discharge Axial Power Distribution vs Measured La <sup>140</sup> Activity for Bundles CX0412, CX0106, CX0394, CX0717, GEB008, and CX0015	225
A-85	Discharge Axial Power Distribution vs Measured La <sup>140</sup> Activity for Bundles CX0498, CX0359, CX0414, CX0191, CX0137, and CX0711	226
A-86	Discharge Axial Power Distribution vs Measured La <sup>140</sup> Activity for Bundles GEB123, CX0316, CX0546, CX0398, CX0286, and CX0057	227

A-87	Discharge Axial Power Distribution vs Measured La <sup>140</sup> Activity for Bundles CX0482, CX0150, CX0719, CX0672, CX0662, AND CX0318	228
A-88	Discharge Axial Power Distribution vs Measured La <sup>140</sup> Activity for Bundles CX0044, CX0523, CX0225, CX0165, GEH022, and CX0396	229
A-89	Discharge Axial Power Distribution vs Measured La <sup>140</sup> Activity for Bundles CX0617, CX0332, GEB132, CX0096, CX0306, and GEH029	230
A-90	Discharge Axial Power Distribution vs Measured La <sup>140</sup> Activity for Bundles CX0231, CX0124, CX0622, GEH023, GEB149, and CX0393	231
A-91	Discharge Axial Power Distribution vs Measured La <sup>140</sup> Activity for Bundles CX0553, CX0401, CX0198, CX0310, CX0024, and CX0186	232
A-92	Discharge Axial Power Distribution vs Measured La <sup>140</sup> Activity for Bundles CX0660, CX0399, CX0093, GEH002, CX0378, and CX0494	233
A-93	Discharge Axial Power Distribution vs Measured La <sup>140</sup> Activity for Bundles CX0575, CX0174, CX0588, CX0287, CX0214, and CX0682	234
A-94	Discharge Axial Power Distribution vs Measured La <sup>140</sup> Activity for Bundles CX0453, CX0490, GEB158, GEB159, GEB160, and GEB161	235
A-95	Predicted vs Measured Local La <sup>140</sup> Activity for Bundle GEB159 at 15" Above Bottom of Active Fuel . . . . .	236
A-96	Predicted vs Measured Local La <sup>140</sup> Activity for Bundle GEB159 at 21" Above Bottom of Active Fuel . . . . .	237
A-97	Predicted vs Measured Local La <sup>140</sup> Activity for Bundle GEB159 at 51" Above Bottom of Active Fuel . . . . .	238
A-98	Predicted vs Measured Local La <sup>140</sup> Activity for Bundle GEB159 at 56" Above Bottom of Active Fuel . . . . .	239
A-99	Predicted vs Measured Local La <sup>140</sup> Activity for Bundle GEB159 at 87" Above Bottom of Active Fuel . . . . .	240
A-100	Predicted vs Measured Local La <sup>140</sup> Activity for Bundle GEB159 at 93" Above Bottom of Active Fuel . . . . .	241
A-101	Predicted vs Measured Local La <sup>140</sup> Activity for Bundle GEB159 at 123" Above Bottom of Active Fuel . . . . .	242

## LIST OF TABLES

B-1	Summary of Peach Bottom TIP Benchmarks . . . .	283
-----	--	-----

## LIST OF FIGURES

B-1	Peach Bottom Unit 2 Core Configuration .	284
B-2	Peach Bottom Unit 2 Critical Eigenvalue Calculated by SIMULATE-E . . . . .	285
B-3	TIP Predictions vs Measurements, Peach Bottom 2 Cycle 1, April 5, 1974 . . . . .	286
B-4	Predicted vs Measured TIP Integrals, Peach Bottom 2 Cycle 1, April 5, 1974 . . . . .	287
B-5	TIP Predictions vs Measurements, Peach Bottom 2 Cycle 1, April 25, 1974 . . . . .	288
B-6	Predicted vs Measured TIP Integrals, Peach Bottom 2 Cycle 1, April 25, 1974 . . . . .	289
B-7	TIP Predictions vs Measurements, Peach Bottom 2 Cycle 1, May 26, 1974 . . . . .	290
B-8	Predicted vs Measured TIP Integrals, Peach Bottom 2 Cycle 1, May 26, 1974 . . . . .	291
B-9	TIP Predictions vs Measurements, Peach Bottom 2 Cycle 1, June 19, 1974 . . . . .	292
B-10	Predicted vs Measured TIP Integrals, Peach Bottom 2 Cycle 1, June 19, 1974 . . . . .	293
B-11	TIP Predictions vs Measurements, Peach Bottom 2 Cycle 1, September 10, 1974 . . . . .	294
B-12	Predicted vs Measured TIP Integrals, Peach Bottom 2 Cycle 1, September 10, 1974 . . . . .	295
B-13	TIP Predictions vs Measurements, Peach Bottom 2 Cycle 1, October 4, 1974 . . . . .	296
B-14	Predicted vs Measured TIP Integrals, Peach Bottom 2 Cycle 1, October 4, 1974 . . . . .	297
B-15	TIP Predictions vs Measurements, Peach Bottom 2 Cycle 1, November 21, 1974 . . . . .	298
B-16	Predicted vs Measured TIP Integrals, Peach Bottom 2 Cycle 1, November 21, 1974 . . . . .	299
B-17	TIP Predictions vs Measurements, Peach Bottom 2 Cycle 1, January 6, 1975 . . . . .	300
B-18	Predicted vs Measured TIP Integrals, Peach Bottom 2 Cycle 1, January 6, 1975 . . . . .	301
B-19	TIP Predictions vs Measurements, Peach Bottom 2 Cycle 1, February 3, 1975 . . . . .	302

B-20	Predicted vs Measured TIP Integrals, Peach Bottom 2 Cycle 1, February 3, 1975 . . . . .	303
B-21	TIP Predictions vs Measurements, Peach Bottom 2 Cycle 1, March 13, 1975 . . . . .	304
B-22	Predicted vs Measured TIP Integrals, Peach Bottom 2 Cycle 1, March 13, 1975 . . . . .	305
B-23	TIP Predictions vs Measurements, Peach Bottom 2 Cycle 1, April 2, 1975 . . . . .	306
B-24	Predicted vs Measured TIP Integrals, Peach Bottom 2 Cycle 1, April 2, 1975 . . . . .	307
B-25	TIP Predictions vs Measurements, Peach Bottom 2 Cycle 1, April 24, 1975 . . . . .	308
B-26	Predicted vs Measured TIP Integrals, Peach Bottom 2 Cycle 1, April 24, 1975 . . . . .	309
B-27	TIP Predictions vs Measurements, Peach Bottom 2 Cycle 1, May 13, 1975 . . . . .	310
B-28	Predicted vs Measured TIP Integrals, Peach Bottom 2 Cycle 1, May 13, 1975 . . . . .	311
B-29	TIP Predictions vs Measurements, Peach Bottom 2 Cycle 1, October 31, 1975 . . . . .	312
B-30	Predicted vs Measured TIP Integrals, Peach Bottom 2 Cycle 1, October 31, 1975 . . . . .	313
B-31	TIP Predictions vs Measurements, Peach Bottom 2 Cycle 1, January 15, 1976 . . . . .	314
B-32	Predicted vs Measured TIP Integrals, Peach Bottom 2 Cycle 1, January 15, 1976 . . . . .	315
B-33	TIP Predictions vs Measurements, Peach Bottom 2 Cycle 1, February 14, 1976 . . . . .	316
B-34	Predicted vs Measured TIP Integrals, Peach Bottom 2 Cycle 1, February 14, 1976 . . . . .	317
B-35	TIP Predictions vs Measurements, Peach Bottom 2 Cycle 1, March 26, 1976 . . . . .	318
B-36	Predicted vs Measured TIP Integrals, Peach Bottom 2 Cycle 1, March 26, 1976 . . . . .	319
B-37	TIP Predictions vs Measurements, Peach Bottom 2 Cycle 2, June 28, 1976 . . . . .	320
B-38	Predicted vs Measured TIP Integrals, Peach Bottom 2 Cycle 2, June 28, 1976 . . . . .	321
B-39	TIP Predictions vs Measurements, Peach Bottom 2 Cycle 2, July 14, 1976 . . . . .	322
B-40	Predicted vs Measured TIP Integrals, Peach Bottom 2 Cycle 2, July 14, 1976 . . . . .	323
B-41	TIP Predictions vs Measurements, Peach Bottom 2 Cycle 2, Sept. 1, 1976 . . . . .	324
B-42	Predicted vs Measured TIP Integrals, Peach Bottom 2 Cycle 2, September 1, 1976 . . . . .	325

B-43	TIP Predictions vs Measurements, Peach Bottom 2 Cycle 2, October 8, 1976 . . . .	326
B-44	Predicted vs Measured TIP Integrals, Peach Bottom 2 Cycle 2, October 8, 1976 . . . .	327
B-45	TIP Predictions vs Measurements, Peach Bottom 2 Cycle 2, October 28, 1976 . . . .	328
B-46	Predicted vs Measured TIP Integrals, Peach Bottom 2 Cycle 2, October 28, 1976 . . . .	329
B-47	TIP Predictions vs Measurements, Peach Bottom 2 Cycle 2, December 16, 1976 . . . .	330
B-48	Predicted vs Measured TIP Integrals, Peach Bottom 2 Cycle 2, December 16, 1976 . . . .	331
B-49	TIP Predictions vs Measurements, Peach Bottom 2 Cycle 2, December 28, 1976 . . . .	332
B-50	Predicted vs Measured TIP Integrals, Peach Bottom 2 Cycle 2, December 28, 1976 . . . .	333
B-51	TIP Predictions vs Measurements, Peach Bottom 2 Cycle 2, January 19, 1977 . . . .	334
B-52	Predicted vs Measured TIP Integrals, Peach Bottom 2 Cycle 2, January 19, 1977 . . . .	335
B-53	TIP Predictions vs Measurements, Peach Bottom 2 Cycle 2, January 26, 1977 . . . .	336
B-54	Predicted vs Measured TIP Integrals, Peach Bottom 2 Cycle 2, January 26, 1977 . . . .	337
B-55	TIP Predictions vs Measurements, Peach Bottom 2 Cycle 2, February 2, 1977 . . . .	338
B-56	Predicted vs Measured TIP Integrals, Peach Bottom 2 Cycle 2, February 2, 1977 . . . .	339
B-57	TIP Predictions vs Measurements, Peach Bottom 2 Cycle 2, February 23, 1977 . . . .	340
B-58	Predicted vs Measured TIP Integrals, Peach Bottom 2 Cycle 2, February 23, 1977 . . . .	341
B-59	TIP Predictions vs Measurements, Peach Bottom 2 Cycle 2, March 11, 1977 . . . .	342
B-60	Predicted vs Measured TIP Integrals, Peach Bottom 2 Cycle 2, March 11, 1977 . . . .	343
B-61	TIP Predictions vs Measurements, Peach Bottom 2 Cycle 2, April 3, 1977 . . . .	344
B-62	Predicted vs Measured TIP Integrals, Peach Bottom 2 Cycle 2, April 3, 1977 . . . .	345

Table C-3  
Summary of River Bend Cold Criticals

Cycle 1

<u>Case</u>	<u>CAVEX (Gwd/T)</u>	<u>Keff</u>	<u>Moderator Temperature</u>	<u>Core Pressure</u>	<u>Rod Density</u>
1	0.000	1.00039	120	15	70
2	0.821	1.01318	466	495	42
3	1.355	1.01041	428	440	45
4	1.384	1.01126	180	15	66
5	2.284	1.00099	487	640	46
6	2.284	1.01057	435	300	48
7	3.027	1.01017	162	15	64
8	3.899	1.00969	285	57	59
9	7.322	1.00701	210	15	58

Cycle 2

<u>Case</u>	<u>CAVEX (Gwd/T)</u>	<u>Keff</u>	<u>Moderator Temperature</u>	<u>Core Pressure</u>	<u>Rod Density</u>
10	7.488	1.01171	130	15	71
11	7.488	1.00949	220	18	71
12	7.488	1.00964	195	15	70
13	7.800	1.00746	502	712	47
14	8.201	1.00978	463	500	57
15	8.324	1.01200	479	552	45
16	8.615	1.00999	437	405	52
17	13.076	1.01594	440	530	64
18	13.283	1.01711	480	920	55
19	13.723	1.01503	205	15	72
20	16.595	1.01244	272	30	71
21	16.639	1.01513	412	525	47

Cycle 3

<u>Case</u>	<u>CAVEX (Gwd/T)</u>	<u>Keff</u>	<u>Moderator Temperature</u>	<u>Core Pressure</u>	<u>Rod Density</u>
22	10.311	1.01021	473	15	83
23	10.394	1.00519	224	415	65
24	11.299	1.00369	370	15	76
25	12.489	1.00543	180	489	58
26	13.956	1.00104	435	19	76
27	16.664	1.01100	152	574	63